Soft Matter

Cite this: *Soft Matter*, 2012, **8**, 3180

www.rsc.org/softmatter

PAPER

Isotactic polystyrene nanorods with gradient crystallite states

Hui Wu,[a] Zhaohui Su[b] and Atsushi Takahara*[acd]

Received 5th October 2011, Accepted 4th January 2012
DOI: 10.1039/c2sm06896f

In this paper, isotactic polystyrene (iPS) nanorods with gradient crystallite distribution were demonstrated. The polymer nanorods with a diameter of 65 nm were prepared by melt-wetting the nanoporous alumina template with fractionated iPS melts. Spatial distribution of crystallinity and orientation of the polymer in the nanorods from top to bottom were analyzed by Fourier transform infrared spectroscopy. The crystallites with perpendicular orientation (*c*-axis perpendicular to the long axis of rod) increased from the top to the bottom of the nanorods due to crystallization initiated by nuclei formed in the bulk and subsequent crystallite growth constrained by the nanopores. This result offers a unique approach to design polymeric nanomaterials with gradient crystallite distribution for functional nanodevice applications.

Introduction

Over the past decade one-dimensional (1-D) polymeric nanomaterials have drawn significant attention due to their unusual properties for potential applications in the fields of storage, separation and catalysis.[1,2] Novel 1-D nanostructures with specific orientation,[3–14] polymorphism,[15] phase-separated morphology,[16,17] anisotropic surface,[18] and gradient composition distribution[19,20] have been demonstrated. Because the physicochemical properties of nanomaterials strongly depend on their morphology, the formation processes, such as annealing temperature and degree of confinement, are commonly used to control the final fine nanostructures.[1–23] For instance, when semicrystalline polymer nanocylinders crystallize at high temperatures, reduced crystallinity[3,4] compared to the bulk and high degrees of orientation[3–13] can be achieved. Whereas for polymeric nanocylinders crystallized at low temperatures, the same crystallinity as that of the bulk and random orientation are obtained.[3,5] As the degree of confinement increases, phase-separated block copolymers in cylindrical nanopores exhibit novel morphologies quite different from that in the bulk.[16,17] The crystallization of polymer is suppressed by decreasing the pore size, and completely stops inside pores with diameters below 20 nm.[22]

Generally, these 1-D nanoobjects are considered to be of uniform structure along the length direction due to the same processes that the whole objects experience. However, the high aspect ratio (length/diameter) of 1-D nanomaterials opens opportunities to anisotropic structures and properties, such as gradient refractive index, improved strength against thermal stress, gradient mechanical modulus and extraordinary plasticity,[24] for the application in functional optical and mechanical nanodevices. To explore these kinds of novel nanomaterial, using isotactic polystyrene (iPS) as an example, polymer nanorods were generated by melt-wetting the nanoporous anodic aluminium oxide (AAO) template with polymer melts. To assess the composition distribution along the length direction of the nanorod, crystallinity and orientation of iPS at different positions of nanorods were investigated by micro-Fourier transform infrared spectroscopy (micro-FTIR), which yields structural information in small sections of the nanorods from top to bottom with spatial resolution. 1-D polymer nanorods with gradient crystallite distribution are demonstrated here.

Experimental

Sample preparation

iPS was kindly supplied by Idemitsu Kosan Co., Ltd. Molecular weight distribution can lead to gradient molecular composition,[19–21] and to minimize this effect on the crystallization behavior of polymer[25] in nanopores, the received polymer was fractionated by successive precipitation using toluene as solvent and methanol as nonsolvent,[26,27] and then by a recycling preparative HPLC (Japan Analytical Industry Co., Ltd., LC-9104) equipped with an RI detector (JAI RI-7s) using $CHCl_3$ as eluent. The polymer with a M_n of 121 000 and a polydispersity of 1.16 (determined by gel permeation chromatography using polystyrene standards) was obtained. The isotacticity was about

[a]*Institute for Materials Chemistry and Engineering, Kyushu University, 744 Motooka, Nishi-ku, Fukuoka, 819-0395, Japan. E-mail: takahara@cstf.kyushu-u.ac.jp*
[b]*State Key Laboratory of Polymer Physics and Chemistry, Changchun Institute of Applied Chemistry, Chinese Academy of Sciences, Changchun, Jilin, 130022, P. R. China*
[c]*JST ERATO Takahara Soft Interfaces Project, CE80, 744 Motooka, Nishi-ku, Fukuoka, 819-0395, Japan*
[d]*International Institute for Carbon-Neutral Energy Research (WPI-I²CNER), Kyushu University, 744 Motooka, Nishi-ku, Fukuoka, 819-0395, Japan*

100% as determined by ^{13}C NMR. AAO templates with a pore diameter of 65 nm and a length of 140 μm were prepared by a two-step electrochemical anodization process using oxalic acid as the electrolyte.[28]

To prepare iPS nanorods, an amorphous polymer film with a thickness of *ca.* 200 μm was obtained by compression-molding the fractionated iPS powder between sheets of aluminium foil under vacuum at 533 K for 4 min and quickly quenching the film in ice water. Then, a porous AAO template was placed on top of the iPS film, and the AAO/iPS assembly was maintained at 533 K for 5 h under vacuum. To achieve the highest degree of crystallinity of iPS, the polymer/AAO assembly was allowed to crystallize at 443 K for 40 h and then quickly quenched in ice water.[29] Thin slices of *ca.* 40 μm thickness of the iPS film with protruding nanorods for SEM and micro-FTIR measurements were obtained by cutting the sample along the rod direction using a razor blade after removal of the AAO template by phosphoric acid solution.

Characterization

A scanning electron microscope (Hitachi S-4300SE) with an accelerating voltage of 5 kV was used to investigate the AAO template and the iPS nanorods. Samples were coated with a thin layer of osmium before performing SEM measurements. Micro-FTIR measurements on the thin slices of iPS nanorods/film were performed on a PerkinElmer Spectra One spectrometer in connection with a microscope equipped with a MCT detector operating in the transmission mode. During the measurements the spatial resolution was 300 × 25 μm^2. Polarized FTIR spectra were recorded using a wire-grid polarizer parallel or perpendicular to the rod direction. All spectra were collected at 2 cm^{-1} resolution with 128 scans co-added. Optical micrographs of iPS nanorods/film under crossed polarizers were taken with a Nikon Eclipse LV100pol microscope, and the images were recorded using a Lumix GH2 camera.

Results and discussion

The iPS nanorods were prepared by wetting the porous AAO templates with polymer melts. The AAO template consists of well-ordered straight separated cylindrical nanopores, and the thermal stability and mechanical rigidity of the alumina wall provide a strictly constrained environment and avoid the breakdown of the cylindrical confinement, offering an effective and convenient template for the preparation of 1-D polymer nanostructures with high aspect ratio. Because the low-energy iPS melts can wet the high-energy nanopore surfaces easily, a capillary rise of iPS melt into the cylindrical nanopores leads to the formation of polymer nanorods.[3] Due to the slow crystallization rate of iPS, the polymer/AAO assembly was allowed to crystallize at 443 K for 40 h to achieve the highest degree of crystallinity.[29] Fig. 1 shows the SEM images of the AAO template with a pore diameter of 65 nm and the parallel aligned iPS nanorods after removal of the AAO template.

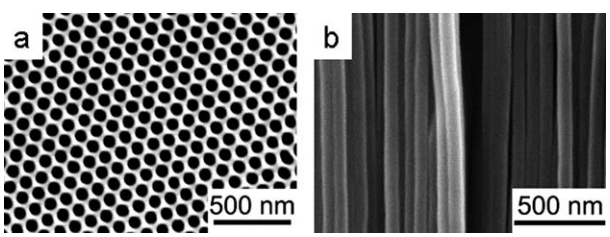

Fig. 1 SEM images of (a) AAO template and (b) iPS nanorods.

Micro-FTIR, the technique as demonstrated in our previous reports,[19,20] was used to characterize the thin slices of iPS nanorods/bulk film obtained by cutting the sample along the rod direction. An optical micrograph and schematic illustration of a thin slice of iPS nanorods/bulk film are shown in Fig. 2A. The dark area at the top is the nanorod array supported by the bulk film, while the translucent section at the bottom is the cross-section of the residual bulk film.[3] The length of the nanorods is about 100 μm. During the FTIR measurements an aperture size of 300 × 25 μm^2 and a resolution of 25 μm along the long axis of the rods were employed to obtain spectra from top to bottom of the thin slice.

Fig. 2B shows the corresponding micro-FTIR spectra of iPS nanorods/film for the measured positions. The top four are the spectra of nanorods at positions *a–d*, while the bottom seven represent the residual bulk film at positions *e–k*, respectively. Band assignments reported in the literature[30–33] are used for the structure analyses. It is known that the band at 1155 cm^{-1} is due to the phenyl CH in-plane deformation.[30] Its intensity does not change substantially during the crystallization process[33] and it has weak dichroism,[31] *i.e.* it is largely unaffected by the crystalline and orientation status. Therefore, the 1155 cm^{-1} band can serve as an internal standard, and all of the data were normalized with respect to this band. The band at 982 cm^{-1} is assigned to CH out-of-plane bending vibration of the phenyl ring,[30,31] which is most sensitive to crystallization with an absorbance increment in proportion to the degree of crystallinity.[34] Hence, the peak height ratio of absorption bands at 982 cm^{-1} and 1155 cm^{-1}, H_{982}/H_{1155}, was used as an indirect index of crystallinity.[27] From Fig. 2B, it can be seen that the intensity of the crystalline band at 982 cm^{-1} increases from position *a* to position *d*, indicating rising crystallinity from the top to the bottom of the nanorods. Thus a gradient crystallinity distribution was formed in the nanorods.

The relative peak heights of the crystalline 982 cm^{-1} band at different positions are plotted in Fig. 3 to better show the variation in crystallinity. The relative peak height from positions *e* to *k* in bulk is almost the same, indicating that the crystallinity in the bulk is uniformly distributed. The relative band intensity in different positions of the nanorods (positions *a–d*) is much weaker than that in the bulk (positions *e–k*), showing that crystallinity in the nanorods is less than that in the bulk, which is in accord with previous reports.[3,4] However, distribution of the crystallinity in the nanorods is not uniform. A steep increase in peak height from position *a* to position *e* is clearly observed, showing that the crystallinity increased rapidly from the top of nanorods to the bulk. The crystallinity of iPS at position *d* is much higher than that at positions *a–c*, indicating the polymer in the nanorods mainly crystallized at the bottom.

Polarized FTIR spectroscopy was then applied to investigate the orientation of the crystalline domains in the sample. The growth direction of the nanorods was defined as the reference direction and polarized FTIR spectra were recorded using a wire-grid polarizer parallel or perpendicular to the rod direction (Fig. 2A). Fig. 2C shows the polarized micro-FTIR spectra at different measured positions of the thin slice. The solid lines are

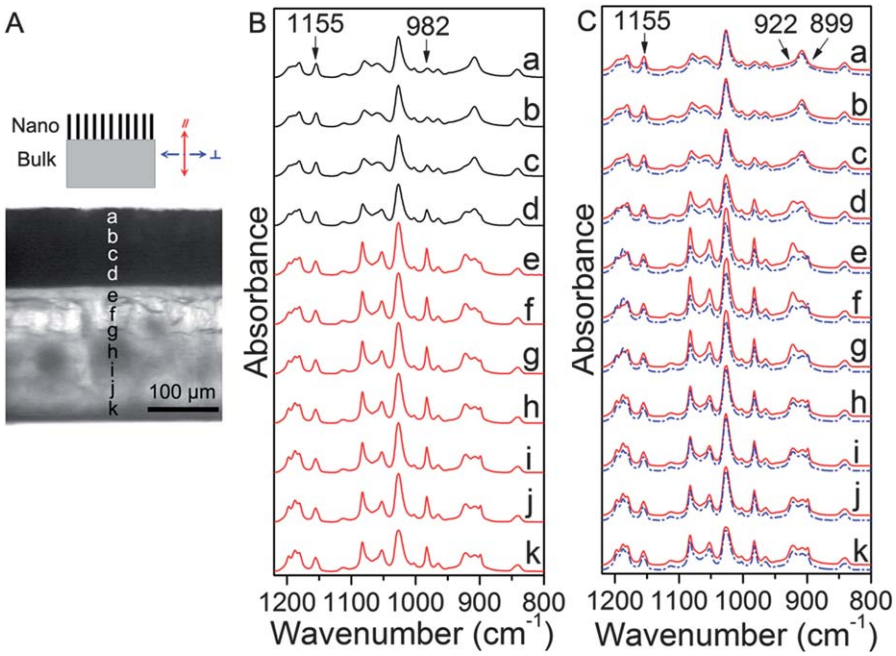

Fig. 2 (A) Optical micrograph and schematic illustration of a thin slice of iPS nanorods/film. The darker section at the top is the nanorod array. (B) Corresponding micro-FTIR spectra at the measured positions. The spatial resolution is 300 × 25 μm² and the spectra are normalized to 1155 cm^{-1} band. (C) Corresponding polarized micro-FTIR spectra at the measured positions: parallel polarization (—) and perpendicular polarization (**---**) with respect to the rod length direction.

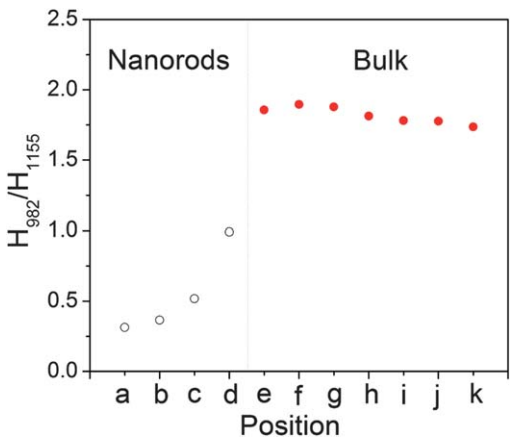

Fig. 3 Normalized peak intensity of the crystalline 982 cm^{-1} band at different positions.

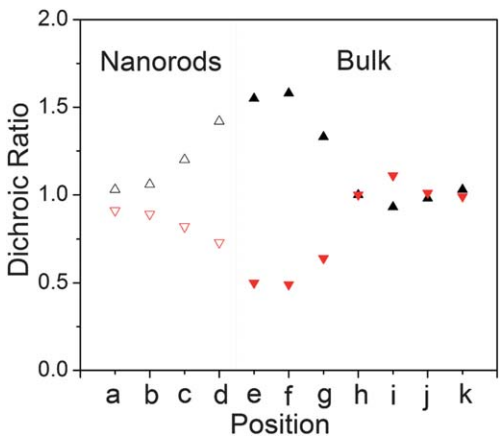

Fig. 4 Dichroic ratio of the 922 cm^{-1} band (△) and 899 cm^{-1} band (▽) at different positions.

the spectra in the parallel polarization, whereas the dashed lines represent the perpendicular spectra. The dichroic ratio of the bands at 922 and 899 cm^{-1} was used to examine the orientation order. These bands were absent in the spectra of the amorphous iPS and are assigned to out-of-plane CH bending vibrations with appropriate perpendicular and parallel dichroism,[30–32] and the IR dichroism of these bands arises from interactions in the crystal lattice rather than isolated chains.[30–32] At the bottom of the nanorods (position *d*), the intensity of 922 cm^{-1} band in the parallel spectrum is stronger than that in the perpendicular one, indicating that the *c*-axis of the crystallites in the nanorods preferentially aligned perpendicular to the rod direction, which is similar to previous results.[3,4,6]

The dichroic ratio of each band was calculated as $R = H_{\parallel}/H_{\perp}$, where $H_{\parallel}$ and $H_{\perp}$ are the measured absorbances (peak height) for electric vector parallel and perpendicular to the rod direction, respectively. Fig. 4 displays the dichroic ratios of the 922 (perpendicular) and 899 cm^{-1} (parallel) bands at different positions in the thin slice, which were extracted from Fig. 2C. For the perpendicular band at 922 cm^{-1}, the dichroic ratio is greater than 1 and increases from position *a* to position *d*, showing that the perpendicular orientation is enhanced from the top to the bottom of the nanorods. Whereas the dichroic ratio of the parallel band at 899 cm^{-1} is less than 1 and decreases from position *a* to position *d*, confirming the results that perpendicular orientation increases from the top to the bottom deduced based on the 922 cm^{-1} band.

It is well known that for melt crystallization in the bulk, polymer crystallization is initiated by heterogeneous nucleation with a relatively small number density of nuclei (defects or impurities extrinsic to the pure material), followed by the dominant three-dimensional spherulitic growth, and finally the whole volume of a semi-crystallized sample is filled completely.[35] Fig. 5 shows an optical micrograph of iPS nanorods/film taken under crossed polarizers. Several black dots in the center of spherulites can be clearly observed in the bulk section, indicating that nuclei formed in the middle of the bulk film. Under the given sampling geometry of 300 × 25 μm^2, polarized FTIR spectra show that the polymer crystallites exhibit almost random orientation at position *h*, and slight parallel orientation at positions *i* and *j*, which verifies the formation of nuclei at positions *h*–*j*. Whereas at positions *e* and *f*, high perpendicular orientation of the polymer crystallites was observed, indicating that the crystallite growth proceeded in a radial fashion with the polymer chain axis being perpendicular to the length of the lamella from each nucleus to positions *e* and *f*, and the growth fronts impinged on the AAO template and the bottom of nanorods at position *d* eventually.

Fig. 6 is a schematic illustration of iPS crystallites developed in the bulk and in the AAO nanopores above to explain the formation of gradient distributed crystallites in the nanorods.

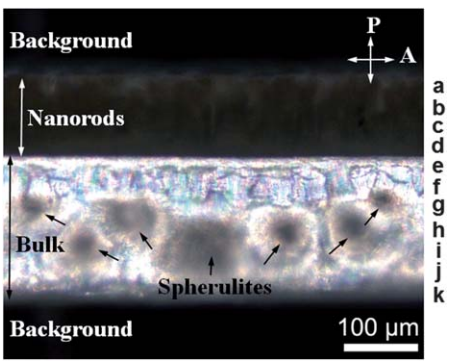

Fig. 5 Optical micrograph of iPS nanorods/film taken under crossed polarizers.

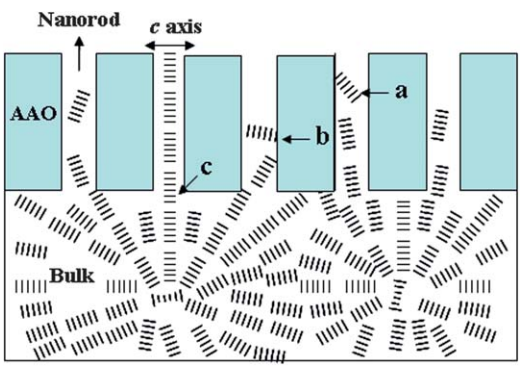

Fig. 6 Schematic illustration of the iPS crystallites developed in AAO nanopores. Three types of nuclei contribute to the crystallization in nanopores: (a) heterogeneous nuclei, which is the same as that in the bulk and of relatively small numbers; (b) nuclei randomly formed at the internal surface of the nanopores; and (c) nuclei formed in the bulk, which play a key role in determining the formation of gradient distributed crystallites in nanopores.

The crystallization of nanorods is mainly governed by the formation of three types of nuclei and the crystallite growth followed. The first type (a in Fig. 6) is heterogeneous nuclei, the same as that in the bulk but there are relatively few. The nanorods can be considered as the bulk polymer being divided into numerous isolated nanometre-sized cylinders by the AAO nanopores. Under the same thermal conditions, the nuclei are randomly distributed among the numerous nanorods with the same density as in the bulk. Because the polymer was filtered in the fractionation process, impurities and particulates were largely removed so that the density of heterogeneous nuclei was very small. This was reflected by the large sizes of the spherulites formed in the bulk. Due to the low density of nuclei and the very small volume of an individual nanorod, few nanorods contain a nucleus statistically and crystallization *via* heterogeneous nucleation only takes place in a tiny portion of the nanorods.[22] Even if a nucleus is present in the isolated nanorods, the cylindrical constraint geometry and limited volume of the nanopores would give rise to frustration of crystallite growth.[6] Once a crystallite begins to grow, transportation of polymer chains between nanorods is hindered due to complete isolation from one another, with only transportation within the nanorod being allowed. Therefore, only the crystallites with growth direction along the long axis of the pore can grow to large sizes, while other growth directions are constrained due to cylindrical confinement of pore walls, which causes a kinetic selection of crystallite growth compatible with the nanopores, leading to crystallites with profound perpendicular orientation.[5,6,9] Hence, numerous polymer nanorods cannot crystallize due to lack of nuclei and they are still in the amorphous state, resulting in much lower crystallinity than that in the bulk. Therefore for the crystallization of separate nanorods, the polymer requires greater supercooling to overcome the intrinsic barrier to nucleation, *i.e.* the crystallization temperature of nanorods is much lower than that of the bulk film.[6,15,22]

The second type (b) is the nuclei randomly formed at the internal surface of the nanopores which have a parallel or near parallel orientation.[7,9] When polymer melt enters the nanopores, the polymer chains are drawn to climb up the nanopore walls by capillary force. The resulting elongational flow promotes partial orientation of chains along the long axis of the nanopores.[7,10] Thus, the extended chain segments would ease the formation of nuclei with *c*-axis parallel to the wall of the nanopores.[7] These nuclei then can develop into crystallites with a parallel or near parallel orientation to decrease the degree of perpendicular orientation. These crystallites are formed in nanopores with statistical frequency at different positions of nanorods from the top to the bottom.

The third type (c) is the nuclei formed in the bulk, which plays a key role in determining the formation of gradient distributed crystallites in the nanorods. In our experiments, the nanorods were connected with a bulk film and the nanorods/bulk experienced the same thermal history. Because of the lack of nuclei in the nanorods, the polymer is difficult to crystallize in the separate nanorods. This offers a good opportunity that the crystallites formed in the bulk can hit the nanorods and serve as nuclei to induce the crystallization of polymer at the bottom of the nanorods (position *d*).[6,7] Due to the 'gate effect' imposed by the nanopores,[6] only crystallites from a fraction of nuclei can grow into the pores to form crystallites with a perpendicular or near

perpendicular orientation. Therefore at the bottom of the nanorods (position *d*) the crystallinity is lower than that of the bulk (positions *e* and *f*) and highly perpendicular orientation is resulted. Because the pore diameter is very small, only the perfectly aligned crystallites can grow into the upper section of the nanorods (positions *c*–*a*), and growth of other not-well aligned crystallites will be stopped by the pore wall. Therefore, the crystallites with perpendicular orientation in the upper parts of the nanorods are much less than that at the bottom and the crystallinity decreases rapidly from the bottom to the top of the nanorods. Combining the contribution of all three types of nuclei, the overall results are that the crystallites with perpendicular orientation decreased from the bottom to the top along the rod direction, and a gradient crystallite distribution is formed in the nanorods.

Conclusions

1-D polymer nanorods with gradient crystallite distribution have been demonstrated. In this study micro-FTIR provided a quantitative tool to assess the chain orientation and crystallinity of polymer in small sections of nanomaterials along the rod direction with satisfactory spatial resolution. The attached bulk and the cylindrical nanopore have pronounced influence over the crystallization process. Due to crystallization initiated by the nuclei formed in the bulk and the constrained crystallite growth in nanopores, crystallites with perpendicular orientation (*c*-axis perpendicular to the long axis of rod) in nanorods decrease from the bottom to the top and the polymer nanorods with gradient crystallite distribution are achieved. This result holds promise for the application of gradient crystallite distributed 1-D nanomaterials to functional optical and mechanical nanodevices in nanotechnology.

Acknowledgements

The present work was supported by a Grant-in-Aid for the Global COE Program "Science for Future Molecular Systems" from the Ministry of Education, Culture, Science, Sports and Technology of Japan. Z.S. thanks the National Natural Science Foundation of China (50921062) for support.

References

1 D. Li and Y. N. Xia, *Adv. Mater.*, 2004, **16**, 1151.
2 M. Steinhart, *Adv. Polym. Sci.*, 2008, **220**, 123.
3 H. Wu, W. Wang, H. Yang and Z. Su, *Macromolecules*, 2007, **40**, 4244.
4 K. Shin, E. Woo, Y. G. Jeong, C. Kim, J. Huh and K. W. Kim, *Macromolecules*, 2007, **40**, 6617.
5 P. Huang, Y. Guo, R. P. Quirk, J. J. Ruan, B. Lotz, E. L. Thomas, B. S. Hsiao, C. A. Avila-Orta, I. Sics and S. Z. D. Cheng, *Polymer*, 2006, **47**, 5457.
6 M. Steinhart, P. Göring, H. Dernaika, M. Prabhukaran, U. Gösele, E. Hempel and T. Thurn-Albrecht, *Phys. Rev. Lett.*, 2006, **97**, 027801.
7 Z. J. Hu, G. Baralia, V. Bayot, J. F. Gohy and A. M. Jonas, *Nano Lett.*, 2005, **5**, 1738.
8 Y. Ma, W. B. Hu, J. Hobbs and G. Reiter, *Soft Matter*, 2008, **4**, 540.
9 H. Wu, W. Wang, Y. Huang and Z. Su, *Macromol. Rapid Commun.*, 2009, **30**, 194.
10 J. Martin, C. Mijangos, A. Sanz, T. A. Ezquerra and A. Nogales, *Macromolecules*, 2009, **42**, 5395.
11 M. C. Garcia-Gutierrez, A. Linares, J. J. Hernandez, D. R. Rueda, T. A. Ezquerra, P. Poza and R. J. Davies, *Nano Lett.*, 2010, **10**, 1472.
12 J. L. Lutkenhaus, K. McEnnis, A. Serghei and T. P. Russell, *Macromolecules*, 2010, **43**, 3844.
13 S. Nojima, Y. Ohguma, K. Kadena, T. Ishizone, Y. Iwasaki and K. Yamaguchi, *Macromolecules*, 2010, **43**, 3916.
14 T. M. Chung, T. C. Wang, R. M. Ho, Y. S. Sun and B. T. Ko, *Macromolecules*, 2010, **43**, 6237.
15 H. Wu, W. Wang, Y. Huang, C. Wang and Z. Su, *Macromolecules*, 2008, **41**, 7755.
16 Y. M. Sun, M. Steinhart, D. Zschech, R. Adhikari, G. H. Michler and U. Gösele, *Macromol. Rapid Commun.*, 2005, **26**, 369.
17 P. Dobriyal, H. Xiang, M. Kazuyuki, J.-T. Chen, H. Jinnai and T. P. Russell, *Macromolecules*, 2009, **42**, 9082.
18 K. Honda, M. Morita, H. Masunaga, S. Sasaki, M. Takata and A. Takahara, *Soft Matter*, 2010, **6**, 870.
19 H. Wu, Z. Su and A. Takahara, *Polym. J.*, 2011, **43**, 600.
20 H. Wu, Z. Su and A. Takahara, *Soft Matter*, 2011, **7**, 1868.
21 M. F. Zhang, P. Dobriyal, J. T. Chen, T. P. Russell, J. Olmo and A. Merry, *Nano Lett.*, 2006, **6**, 1075.
22 H. Duran, M. Steinhart, H. J. Butt and G. Floudas, *Nano Lett.*, 2011, **11**, 1671.
23 O. Azzaroni and K. H. A. Lau, *Soft Matter*, 2011, **7**, 8709.
24 T. H. Fang, W. L. Li, N. R. Tao and K. Lu, *Science*, 2011, **331**, 1587.
25 E. Ergoz, J. G. Fatou and L. Mandelkern, *Macromolecules*, 1972, **5**, 147.
26 F. Danusso and G. Moraglio, *J. Polym. Sci.*, 1957, **24**, 161.
27 K. Kawahara and R. Okada, *J. Polym. Sci.*, 1962, **56**, S7.
28 H. Masuda and K. Fukuda, *Science*, 1995, **268**, 1466.
29 R. Hammel, W. J. MacKnight and F. E. Karasz, *J. Appl. Phys.*, 1975, **46**, 4199.
30 H. Tadokoro, Y. Nishiyama, S. Nozakura and S. Murahashi, *Bull. Chem. Soc. Jpn.*, 1961, **34**, 381.
31 P. C. Painter and J. L. Koenig, *J. Polym. Sci., Part B: Polym. Phys.*, 1977, **15**, 1885.
32 B. Jasse and J. L. Koenig, *Polymer*, 1981, **22**, 1040.
33 T. Kimura, H. Ezure, S. Tanaka and E. Ito, *J. Polym. Sci., Part B: Polym. Phys.*, 1998, **36**, 1227.
34 Y. X. Duan, J. M. Zhang, D. Y. Shen and S. K. Yan, *Macromolecules*, 2003, **36**, 4874.
35 B. Wunderlich, *Macromolecular Physics*, Academic Press, Inc., New York, 1973, vol. 2.

